Sodium channel selectivity and conduction: Prokaryotes have devised their own molecular strategy

Rocio K. Finol-Urdaneta,[1,2] Yibo Wang,[3] Ahmed Al-Sabi,[1,2] Chunfeng Zhao,[3] Sergei Y. Noskov,[3] and Robert J. French[1,2]

[1]Department of Physiology and Pharmacology, [2]Hotchkiss Brain Institute, and [3]Department of Biological Sciences, Institute for Biocomplexity and Informatics, University of Calgary, Calgary, Alberta T2N 4N1, Canada

Striking structural differences between voltage-gated sodium (Nav) channels from prokaryotes (homotetramers) and eukaryotes (asymmetric, four-domain proteins) suggest the likelihood of different molecular mechanisms for common functions. For these two channel families, our data show similar selectivity sequences among alkali cations (relative permeability, Pion/PNa) and asymmetric, bi-ionic reversal potentials when the Na/K gradient is reversed. We performed coordinated experimental and computational studies, respectively, on the prokaryotic Nav channels NaChBac and NavAb. NaChBac shows an "anomalous," nonmonotonic mole-fraction dependence in the presence of certain sodium–potassium mixtures; to our knowledge, no comparable observation has been reported for eukaryotic Nav channels. NaChBac's preferential selectivity for sodium is reduced either by partial titration of its highly charged selectivity filter, when extracellular pH is lowered from 7.4 to 5.8, or by perturbation—likely steric—associated with a nominally electro-neutral substitution in the selectivity filter (E191D). Although no single molecular feature or energetic parameter appears to dominate, our atomistic simulations, based on the published NavAb crystal structure, revealed factors that may contribute to the normally observed selectivity for Na over K. These include: (a) a thermodynamic penalty to exchange one K^+ for one Na^+ in the wild-type (WT) channel, increasing the relative likelihood of Na^+ occupying the binding site; (b) a small tendency toward weaker ion binding to the selectivity filter in Na–K mixtures, consistent with the higher conductance observed with both sodium and potassium present; and (c) integrated 1-D potentials of mean force for sodium or potassium movement that show less separation for the less selective E/D mutant than for WT. Overall, tight binding of a single favored ion to the selectivity filter, together with crucial inter-ion interactions within the pore, suggests that prokaryotic Nav channels use a selective strategy more akin to those of eukaryotic calcium and potassium channels than that of eukaryotic Nav channels.

The Journal of General Physiology

INTRODUCTION

The classic experiments of Hille defined selectivity profiles for voltage-gated sodium (Nav) and potassium channels (Hille, 1971, 1972, 1973), and later for nAChR channels at the neuromuscular junction (Adams et al., 1980). These determinations were based on relative permeability values calculated from shifts in reversal potential determined under voltage clamp. The approach offered a well-defined protocol for comparison of the ease with which different ions entered a particular channel. Such measurements, systematically performed for alkali cations, and a series of variously sized organic cations roughly defined the limits for the size, and to some degree the cross-sectional shape, of the narrowest part of each channel, henceforth known as the "selectivity filter." A similar analysis was performed for voltage-gated Ca channels from skeletal muscle (McCleskey and Almers, 1985). Later, single-channel recording allowed direct comparisons of unitary conductance, measured in the presence of different permeating ions, which provides an alternate indication of channel selectivity (Meech and Mackie, 1993; Thompson et al., 2009). Although, depending on the molecular details of conduction, relative permeabilities and conductances obtained from these two approaches may differ, the analysis of reversal potential shifts resulting from external cation replacement endures as one convenient and widely used approach to measure ion channel selectivity.

Studies on Nav channels from frog node of Ranvier suggested a selectivity filter of asymmetric cross section, measuring a minimum of $\sim 3 \times 5$ Å (Hille, 1971). Subsequently, the selectivity filter was later identified as the highly conserved signature motif, DEKA (see rSkM1 pore sequence fragments in Fig. 1), to which one amino acid residue was contributed by each of the homologous repeat domains of the Nav channel α subunit (Heinemann et al., 1992).

R.K. Finol-Urdaneta and Y. Wang contributed equally to this paper.
Correspondence to Robert J. French: french@ucalgary.ca; or Sergei Y. Noskov: snoskov@ucalgary.ca

Abbreviations used in this paper: Cav, voltage-gated calcium; MD, molecular dynamics; Nav, voltage-gated sodium; PMF, potential of mean force.

The Rockefeller University Press $30.00
J. Gen. Physiol. Vol. 143 No. 2 157–171
www.jgp.org/cgi/doi/10.1085/jgp.201311037

In contrast, Hille's analysis for delayed rectifier K channels suggested a symmetric selectivity filter of ~3 Å in diameter (Hille, 1973). The first crystal structure determined for a K channel revealed a size closely matching this estimate, and showed that the lumen of the selectivity filter was lined by backbone carbonyls (Doyle et al., 1998) of residues from the K channel signature sequence (Heginbotham et al., 1994). In contrast, functional data for Nav and voltage-gated calcium (Cav) channels suggested a filter lumen lined by amino acid side chains providing a net negative charge (Kim et al., 1993; Tang et al., 1993; Yang et al., 1993).

Functional characterization by the Clapham laboratory of a homotetrameric, prokaryotic Nav channel, NaChBac (Ren et al., 2001), prompted hopes for an Nav channel crystal structure. After 10 years, these hopes were realized by Catterall and collaborators (Payandeh et al., 2011, 2012), using the NaChBac relative NavAb, closely followed by Zhang et al. (2012) and McCusker et al. (2012). Studies on these prokaryotic channels shattered the maxim that an asymmetric selectivity motif was required to achieve selectivity for Na^+ over K^+ and common divalent metal ions (Backx et al., 1992; Heinemann et al., 1992). In the prokaryotic Nav channels, sequence alignment and structure are consistent with a selectivity ring made up of one glutamate residue from each of the four monomers, reminiscent of the EEEE selectivity filter of four-domain eukaryotic Cav channels (Fig. 1 D). In eukaryotic Nav channels, there is a conserved outer ring of acidic residues, three to four positions C terminal from the DEKA motif (Fig. 1 D), but this outer ring appears to influence conductance and proton block, rather than determine selectivity (Khan et al., 2002). Although follow-up studies of NaChBac showed that it could easily be converted into a Ca-selective channel by the addition of one or more additional acidic residues into the outer vestibule-lining P loop (Yue et al., 2002), the detailed mechanism by which the NaChBac family of prokaryotic channels achieves Na selectivity with an EEEE selectivity filter has yet to be clarified.

Similar to voltage-gated potassium channels, the NavAb channel is a homotetramer. Each monomer is composed of six transmembrane helices, S1–S6. The first four helices, S1–S4, form the voltage-sensing domain, whereas helices S5 and S6, plus their connecting loop, form the pore domain, through which ions permeate. Notably, the presumed selectivity filter of the NavAb channel is wider than those of K^+ channels. The resolution of the crystal structures renders unambiguous positioning of permeant ions difficult. Nevertheless, up to three binding sites were proposed based on a combination of functional and structural studies (Payandeh et al., 2011). T175 of each monomer forms the inner (cytoplasmic) site, S_{IN}, whereas main-chain oxygens of L176 aided by the water molecules comprise the central site, S_{CEN}, and the acidic side chain of E177 ligates permeant ion in the outermost, high field–strength site, S_{HFS} (Fig. 1 A). The question of how this filter gives rise to selective permeation, including the functional role of the varying polarity among its different binding sites, has yet to be resolved.

The general physical principles underlying selectivity in prokaryotic and eukaryotic Nav channels may be similar, but the molecular details show some striking differences. A broad structural similarity is seen in the asymmetry along the pore axis. Both prokaryotic and eukaryotic Nav channels possess a selective periplasmic, or extracellular, section of the pore, with an outer vestibule that quickly grades into the narrow selectivity filter, followed by an expansive aqueous inner cavity, roughly aligned with the hydrophobic center of the surrounding bilayer, and then, a nonselective cytoplasmic mouth. The points of difference are tantalizing and include, in prokaryotes, the more negative net charge of the EEEE selectivity ring and the radial quasi symmetry, which contrasts with the strongly asymmetric DEKA ring of eukaryotic Nav channels (Fig. 1 D).

Among the eukaryotic members of the P-loop ion channel molecular family, Cav and Kv channels show functional characteristics that are most easily explained if each channel normally accommodates two to four conducting ions. These properties include tight binding of the preferred ion species (Hess and Tsien, 1984; Morais-Cabral et al., 2001), strong coupling of unidirectional ion fluxes through the channel (Hodgkin and Keynes, 1955; Busath and Begenisich, 1982), and a nonlinear dependence of conductance on the mole fraction for mixed-ion solutions (Hille and Schwarz, 1978). In contrast, eukaryotic Nav channels show a saturating dependence of single-channel conductance on sodium concentration with half-maximal conductance in the millimolar range (Hille, 1975b; Moczydlowski et al., 1984; French et al., 1994), very weak flux coupling (Busath and Begenisich, 1982), and other features consistent with only a single ion being bound to the channel most of the time (Ravindran et al., 1992; French et al., 1994). Perhaps the most obvious connection is that, functionally, bacterial Nav channels tend to be leakier to calcium ions than their eukaryotic counterparts, and several point mutations allow them to preferentially conduct calcium (Yue et al., 2002). A key question that we address here is how bacterial Nav channels can show selectivity and conductance closely approximating those of their eukaryotic counterparts, whereas their multi-ion occupancy, suggested by available structures, is more akin to that of eukaryotic Cav and Kv channels.

We experimentally evaluate NaChBac's alkali cation selectivity under a variety of conditions and explore possible mechanistic and molecular underpinnings of that selectivity using computer simulations based on the

related NavAb crystal structure. Although these are two different channels, they display a considerable structural similarity; for example, both channels are homotetramers with high sequence identity, especially in the pore domain. Judging by multiple studies of 2TM and 6TM potassium channels, a wide variety of channels with apparent difference in sequence produces similar structures of the pore domain (within 1–2-Å resolution for backbone atoms).

We identify possible determinants of conduction and alkali cation selectivity of bacterial sodium channels by analysis of molecular dynamics (MD) simulations and calculations of 1- and 2-D potentials of mean force (PMFs) for ions moving within the conducting pore. We find that the functions of selectivity and conduction resemble those of eukaryotic Navs, even though patterns of ion interaction and occupancy are more like those of Cav and, to a lesser extent, Kv channels.

MATERIALS AND METHODS

Mutagenesis

The original NaChBac channel construct in pTracer-CMV2 (Invitrogen) was provided by D. Clapham (Howard Hughes Medical Institute, Children's Hospital, and Harvard University, Boston, MA). Single amino acid mutants were generated as described previously (Light et al., 2000), using overlapping PCR amplification with oligonucleotide containing the sequence for the desired amino acid substitutions, followed by subcloning into pTracer (Invitrogen). All clones were completely sequenced.

Electrophysiology

Mammalian tSA 201 cells (Margolskee et al., 1993) were transfected with DNA encoding WT or mutant NaChBac, plus GFP using Polyfect (QIAGEN). Significant channel expression occurred within 24 h, after which whole-cell patch-clamp recordings were made at room temperature with an amplifier (Axopatch 200B; Molecular Devices). Patch pipettes were pulled from glass (8161; Corning; Potash-Rubium-Lead; softening temperature, 600°C; dielectric constant, 8.3) to a resistance of 1.5–2.5 MΩ. Recordings were made 24 h after transfection in control external solution that contained (mM): 142.5 NaCl, 2 $CaCl_2$, 2 $MgCl_2$, 10 glucose, and 10 HEPES, pH 7.4. External ion replacement solutions were made by substituting 142.5 mM Na by Li, K, Rb, or Cs. Control intracellular (pipette) solution ("Na_{in}") contained (mM): 105 CsF, 35 NaCl, 10 EGTA, and 10 HEPES, pH 7.2. "K_{in}" was made by substituting 35 mM NaCl by 35 mM KCl. For bi-ionic experimental conditions, the intracellular solution contained either 140 mM Na, K, or Cs. External solution changes were achieved by local superfusion of the replacement solution over the cell, with appropriate corrections for changes in junction potential (see Data analysis below).

Data analysis

Data were analyzed using Clampfit (Molecular Devices) and Igor (WaveMetrics) software. Peak I-V curves were fitted using $I(V) = (V - V_{rev}) * G_{max}/(1 + \exp((V_{half} - V)/V_{slope}))$, where I is the macroscopic current, V is the command potential, V_{rev} is the reversal potential, G_{max} is the maximal conductance, V_{half} is the half-activation potential, and V_{slope} is the slope factor (mV/e-fold). For weakly permeant external ions, the reversal potential is expected to occur in a negative voltage range, at which very little conductance is activated (e.g., Fig. 4 C, left, internal sodium, external potassium). Thus, in the presence of weakly permeant ions, a prepulse to −10 mV was applied to induce maximal activation, and V_{rev} was determined from the instantaneous I-V relation, measured from the initial point in the tail current decay after steps to a series of voltages encompassing V_{rev}. For weakly permeant ions, this protocol provided a more precise and reproducible estimate of V_{rev}. Relative permeabilities were calculated according to: $P_X/P_{Na} = \exp((E_X - E_{Na})/(RT/F))$, where P_X is permeability to ion X, P_{Na} is Na permeability, and RT/F is 25.4 mV.

Net junction potentials were balanced to reduce the pipette current to zero before seal formation. In experiments where solution replacement happened after the seal was established, the theoretical junction potential for each solution pair was determined using JPCalc from Clampfit, which was also used for V_{rev} correction before the calculation of the permeability ratio. Series resistance compensation was applied conservatively to favor voltage-clamp stability; we note that the series resistance correction approaches zero near the reversal potential, the most critical measurement in this study. Net junction potential corrections applied to estimates of V_{rev} fell in the range of 1.8–9.9 mV.

All summary data are presented as mean ± SEM (n), where n is the number of determinations. Statistical significance was evaluated using the unpaired Student's t test; the criterion for a significant difference was taken to be $P < 0.05$, unless otherwise stated.

Computational strategies

The initial structure of NavAb was taken from the high resolution x-ray crystallographic structure with the Protein Data Bank accession number 3RVY (Payandeh et al., 2011). The structure corresponds to a closed-pore conformation. The molecular simulations reported in this study were focused on the WT NavAb (Fig. 1 A) and the E177D mutant (Fig. 1 B). The tetrameric channel was embedded into a pre-equilibrated DMPC lipid bilayer and solvated in a 104 × 104 × 80–$Å^3$ box filled with TIP3P water using CHARMM-GUI membrane builder protocol (Jo et al., 2008). The whole assembly was bathed with 150 mM NaCl, ensuring electroneutrality. Although Na^+ ions were not directly observed in the crystallographic structure, three Na^+ ions were positioned in the filter as the starting conformation (as shown in Fig. 1 C), based on continuum electrostatic computations. All MD simulations were performed by the program CHARMM (Brooks et al., 2009). The CHARMM-27 force field was used for protein and lipids (MacKerell et al., 1998; Feller and MacKerrell, 2000), and Na^+ and K^+ ions as reported previously (Noskov et al., 2004; Noskov and Roux, 2008).

The NpT ensemble was used for all simulations, with pressure set to 1 atm and temperature set to 315 K. Long-range electrostatic interactions were treated by the particle mesh Ewald algorithm (Essmann et al., 1995). Nonbonded interactions were switched off at 10–12 Å. The systems were simulated with periodic orthorhombic boundary conditions applied in all directions with the time step of 1 fs. After a staged equilibration with a gradual decrease in harmonic constraints that act on heavy protein atoms only, further nonconstrained equilibration was run for 23 ns.

To unravel energetics of ion permeation, we used multidimensional umbrella sampling methods, a powerful computational technique used with considerable success in studies of K channels. Umbrella sampling simulations were performed with harmonic biasing potentials with a force constant of 10 kcal/(mol · $Å^2$) along the z axis. The zero position along the z axis is the center of mass of the selectivity filter backbone atoms of residues T175, L176, and E177. 1- and 2-D profiles for ions were computed. The lateral displacement of ion(s) was restrained to be within a cylinder with a radius of 10 Å and the central axis along the z axis. The reaction coordinate for each ion was the distance along the z axis between the ion and the center of mass of the selectivity filter of the protein, as just defined. The final snapshots of the conventional MD were used as the starting conformations for the umbrella

sampling. The sampling windows were spaced every 0.5 Å from +14.5 to −10 Å, resulting in 50 windows for 1-D PMF computations and 1,045 windows for 2-D PMFs. The simulation time per window was set to 3 ns for 1-D PMF computations and 0.5 ns for 2-D PMF computations, respectively.

1-D PMFs (e.g., Figs. 3 B and 6 B) were obtained by integration along a pathway for a single ion across a 2-D map (e.g., Fig. 3 C). Such 1-D PMFs, in general, would be expected to trace out a likely low energy pathway of one ion across the 2-D PMF surface, as illustrated in Fig. 3 C, and would reflect the ion's interactions with its environment, including other ions, protein, and solvent. Convergence of computed 1-D PMFs obtained from a 2-D PMF map obtained after simulation times of 100–500 ps is illustrated in Fig. S3. The energy surfaces were rebuilt with the weighted histogram analysis method (WHAM) (Kumar et al., 1992; Grossfield, 2012), and the tolerance for WHAM was set to 0.001.

In some cases, 2-D PMFs were further analyzed by extracting 1-D "cross sections," for which one ion is held constant, whereas the other is moved on a single reaction coordinate across the profile (e.g., Fig. 3 E, and see Results). An indication of the significance of differences between PMFs or profiles of other parameters is given by SEMs estimated from standard block-average calculations (Rapaport, 2004) using progressively increasing block sizes (see Figs. 3, A and D, and 6, A, B, and D and associated text).

The single equilibrium dissociation constant K_D(single) from 1-D PMF in the presence of a cylindrical constraint can be expressed as follows (Allen et al., 2004; Kim and Allen, 2011):

$$K_D^{-1}(single) = \pi R^2 \int_{z_{min}}^{z_{max}} \mathrm{d}z\ \mathrm{e}^{-w(z)/k_BT}, \qquad (1)$$

where R is the radius of the cylindrical restraint oriented normal to the z axis with $z_{min} = -10$ Å and $z_{max} = 14.5$ Å. The $w(z)$ was offset to zero for an ion in the bulk phase.

The equilibrium dissociation constant for the double occupancy state of the channel, K_D(double), can be expressed in accordance with Allen et al. (2004):

$$K_D^{-1}(double) = \frac{(\pi^2 R^4)\int_{z_{1,min}}^{z_{1,max}} \mathrm{d}z_1 \int_{z_{2,min}}^{z_{2,max}} \mathrm{d}z_2\ \mathrm{e}^{-w(z_1,z_2)/k_BT}}{\pi R^2 \int_{z_{min}}^{z_{max}} \mathrm{d}z\ \mathrm{e}^{-w(z)/k_BT}}, \qquad (2)$$

with the following integration limits: -7 Å ≤ z_1 ≤ 20 Å and -10 Å ≤ z_2 ≤ 20 Å.

Online supplemental material

The supplemental figures provide additional experimental data to complement that presented in the main text, as follows. Fig. S1 illustrates the time courses of wash-in and washout, as K^+ replaces Na^+ in the external solution. Combined with the results in the main text, Fig. 2 (A–C), the data make two points: (1) washout of K^+, and its replacement by Na^+, is significantly slower than the reverse, suggesting stronger binding of K^+ under these conditions; and (2) washout of K^+, in particular, depends significantly on the complement of intracellular ions, with the slowest being observed with intracellular solutions containing Cs^+ or Na^+ as the sole internal alkali cation species. Fig. S1 shows that no anomalous mole-fraction dependence is seen when external Na^+ is replaced by K^+, with intracellular media containing 105 mM Cs^+ with 35 mM K^+ or Na^+. This contrasts sharply with the observations for intracellular

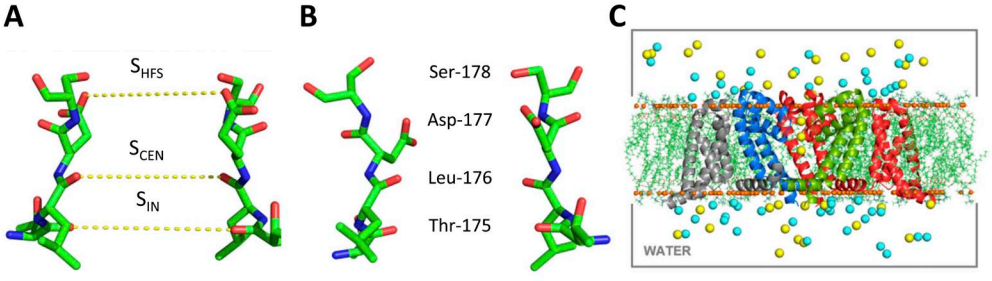

D

		P1	SF	P2	Ident	Simil	Q_{SF}
NaChBac	173	YFGNLQLSLLTLFQVVTLESWASGVMRPIFAEVWWS			208	100	100	−4
NavAb	159	WFGTLGESFYTLFQVMTLESWSMGIVRPLMEVYPYA			194	61	79	−4
NavRh	161	SRWDLGISLITLFQVLTLSSWETVMLPMQEIYWWSW			196	55	73	−4
rSkM1-DI	382	SYDTFSWAFLALFRLMTQDYWENLFQLTLRAAGKTY			417	31	69	−5
rSkM1-DII	737	HMNDFFHSFLIVFRILTGEWIETMWDCMEVAGQAMC			772	0	0	
rSkM1-DIII	1119	NYDNVGLGYLSLLQVATFKGWMDIMYAAVDSREKEQ			1154	0	0	
rSkM1-DIV	1510	FNFETFGNSICLFEITTSAGWDGLLNPILNSGPPDC			1545	0	0	
hCav1.2-DI	345	NFDNFAFAMLTVFQCITMEGWTDVLYWMQDAMGYEL			380	41	64	−8
hCav1.2-DII	688	TFDNFPQSLLTVFQILTGEDWNSVMYDGIMAYGGPS			723	47	60	
hCav1.2-DIII	1117	DFDNVLAAMMALFTVSTFEGWPELLYRSIDSHTEDK			1152	36	54	
hCav1.2-DIV	1446	NFQTFPQAVLLPLRCATGEAWQDIMLACMPGKKCAP			1478	0	0	
Shaker	423	NSFFKSIPDAFWWAVVTMTTVGYGDMTPVGVWGKIV			458	40	60	0
KvAP	177	NSSIKSVFDALWWAVVTATTVGYGDVVPATPIGKVI			212	0	0	0

Figure 1. Pore domains for prokaryotic and eukaryotic Nav, Cav, and voltage-gated potassium channels. (A) Proposed locations of ion-binding sites in the selectivity filter of WT NavAb (Payandeh et al., 2011) and (B) the corresponding organization of the selectivity filter in the NavAb E177D mutant. (C) NavAb crystal structure modeled within a DMPC lipid bilayer (see Materials and methods) showing the permeation pathway lined by the selectivity filter. The nearest voltage-sensing domain and pore domain, and the farthest voltage-sensing domain, are removed for clarity. Chloride and sodium ions are shown as cyan and yellow spheres, respectively. The lipid phosphate groups are represented by orange spheres. The simulated aqueous phase is bounded by the gray lines. (D) Comparison of pore domain sequences among prokaryotic and eukaryotic voltage-gated cation channels (P1, pore helix 1; SF, selectivity filter; P2, pore helix 2). Ident, percent identity; Simil, percent aligned similar residues compared to NaChBac. Note that Q_{SF}, the net charge on the selectivity filter, includes both inner and outer charged rings in the eukaryotic sodium and calcium channels. The rat skeletal muscle sodium channel, rSkM1, is also known as rNav1.4.

solutions containing either only K^+ or only Na^+, which reveal a dramatic anomalous mole-fraction dependence (Fig. 4 D). Fig. S2 provides voltage-clamp records from NaChBac E191D taken at extracellular pH values of 7.4 and 5.8. Even though the E191D mutant is much less selective for Na^+ over K^+ than is the WT channel, an additional significant loss of selectivity (i.e., an increase in P_K/P_{Na}) was observed with a decrease of extracellular pH (Fig. 5 B). Fig. S3 illustrates convergence of a 1-D PMF computed from a 2-D map. The online supplemental material is available at http://www.jgp.org/cgi/content/full/jgp.201311037/DC1.

RESULTS

Overview

In this Results section, we stress the overriding goal of our study: to systematically integrate experimental and computational results that suggest the mechanisms underlying selectivity among alkali cations by bacterial Nav channels, exemplified by NaChBac and NavAb. To this end, we interleave results from experiments and simulations throughout. We begin with the classic approach of measuring relative permeabilities, based on reversal potential shifts observed when the external cation species is changed, and calculations of the PMF as a single ion is moved through the channel. Intuitively, one might expect that reversal potential shifts generated by external ion substitution are expected to be primarily influenced by the energetics of ion entry into the pore (Patlak, 1960; Bezanilla and Armstrong, 1972), and hence by the outermost parts of the pore structure. It is this part of the pore structure that is likely to differ least between open and closed conformations in channels for which control of channel opening is presumed to lie at the S6 bundle crossing on the cytoplasmic side of the selectivity filter. Thus, we believe that the putative preopen structure of Payandeh et al. (2011) is an appropriate basis for a consideration of selectivity based on relative permeability measurements.

Subsequently, we present experimental results observed after changes in the ion species on both extracellular and intracellular sides of the membrane. These experiments are more likely to yield results indicating whether or not ion–ion interactions play a prominent role in ion selectivity and conduction. Their analysis required simulations

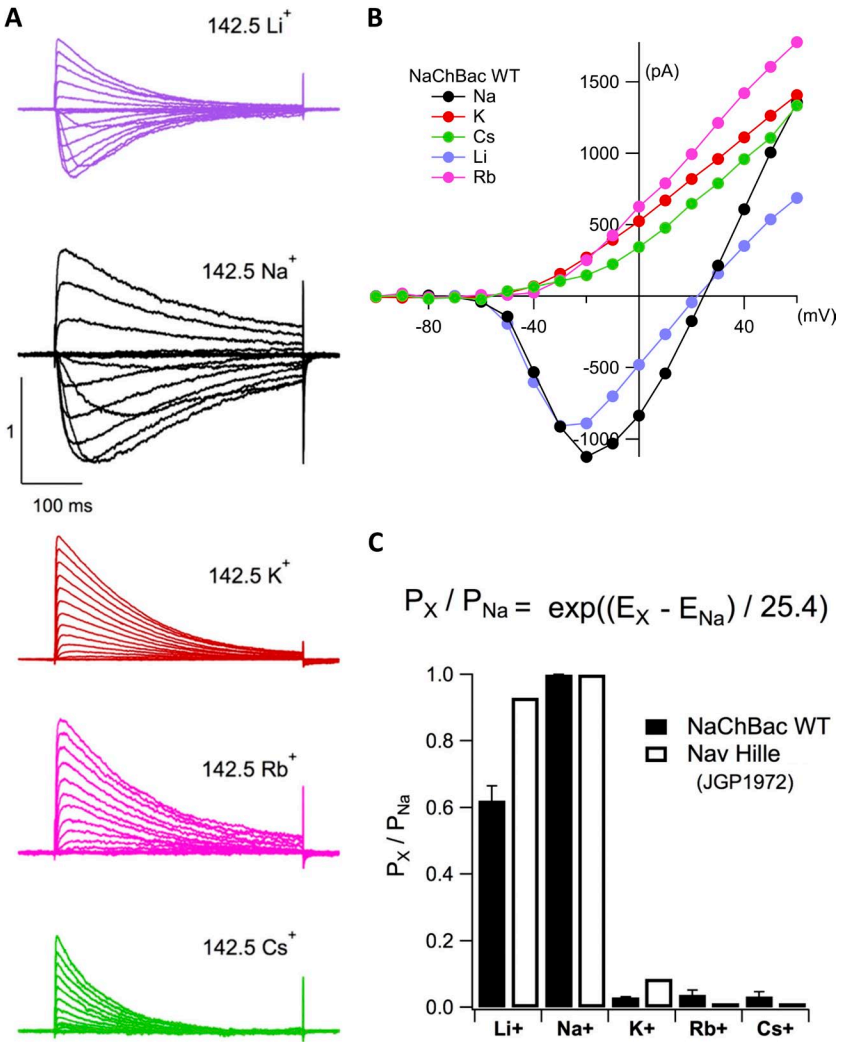

Figure 2. NaChBac relative permeabilities to alkali cations show the same sequence as for eukaryotic Nav channels, with small quantitative differences for some individual ions. (A) Whole-cell NaChBac-mediated currents in the presence of different extracellular alkali cations. Current amplitudes for the substituted ions are normalized to the maximum inward sodium current in the same cell. (B) Representative I-V relationships for each cation substitution shown in A. Ordinate values show current amplitudes with 142.5 mM of external Na; for other ions, currents are normalized as in A. (C) Relative permeabilities, from I-V reversal potential shifts after external cation substitutions, calculated using the equation shown. Closed bars, with error bars, correspond to NaChBac data, and open bars show relative permeability of frog node of Ranvier Na channels, as reported by Hille (1972).

in which at least two ions occupy the channel, which led us to explore the implications of the resulting 2-D PMFs that emerge (see below).

Relative permeability fingerprint

The qualitative selectivity fingerprint (Fig. 2), defined by the sequence of relative permeability values, P_X, where P_{Na} is defined as 1, matches both the sequences determined from similar experiments for eukaryotic Nav channels (e.g., Hille, 1972) and the sequence for equilibrium binding to high field–strength anionic sites (Eisenman, 1962). Our experiments used 105 mM Cs as the major internal cation with 35 mM of internal Na to allow easy measurement of either positive or negative shifts in Erev, with a quasi-physiological inward electrochemical gradient for Na over most of the working experimental voltage range. The resulting selectivity sequence is $P_{Li} \sim P_{Na} > P_K \approx P_{Rb} \approx P_{Cs}$.

Moving ions through the pore: PMFs for single and double occupancy

As a first step toward defining the energetics of ion permeation, we evaluated 1-D PMFs as single ions were moved through the NavAb model pore (Fig. 3 A). In the absence of other ions, a solitary Na^+ would bind much too tightly to permit physiological rates of throughput (single-channel conductance, ~12 pS or $\sim 10^7$ ions/s^{-1}, with a 100-mV driving force; Ren et al., 2001). From the

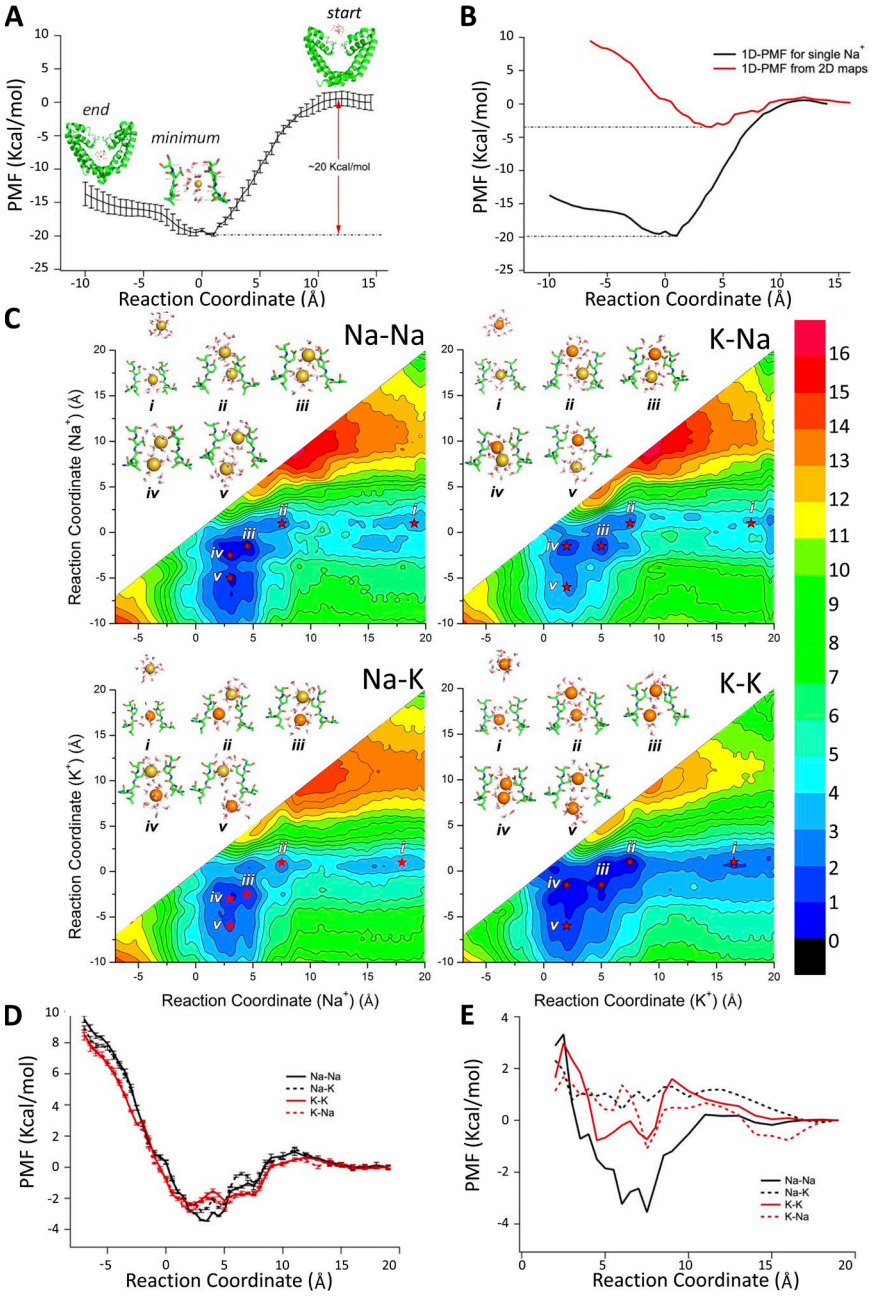

Figure 3. Calculated energy profiles and contour maps, for single-ion and two-ion pore occupancy, which determine the movement of ions across the NavAb pore. (A) 1-D potential of PMF for the movement of a single Na^+ ion across the selectivity filter of NavAb. Note that single-ion binding would be much too tight to permit the experimentally observed conductances. (B) Superposition of 1-D PMFs for movement of a single Na^+ ion in the cases of single and double occupancy (see low energy pathway, *i–v* in C, Na–Na case.). For double occupancy, the barrier for ion exit back to the extracellular solution is drastically reduced, reflecting weaker binding and allowing larger conductance. (C) 2-D PMFs for the movement of two ions, Na^+ and/or K^+, as indicated, with labeled points (*i–v*) shown along the lowest energy permeation pathway. Na–Na and K–Na describe the plots where a Na^+, or a K^+ ion, moves in the presence of a Na^+ ion. K–K and Na–K are plots where K^+ or Na^+ moves in the presence of a K^+ ion. In every case, both ions were free to move, as indicated in the insets. (D) 1-D PMFs for different double-occupancy combinations from the 2-D contour plots shown in C: Na–Na, K–K, K–Na, and Na–K. Each profile was obtained by integration from the 2-D PMF maps (see Materials and methods). (E) 1-D cross sections of 2-D PMFs for different double-ion occupancy of the selectivity filter, when one ion is fixed at the position of binding site *ii*, (see C). The cross sections illustrate the energy scape experienced by the second ion-entering selectivity filter. As is apparent from the differences between D and E, significant energetic differences arise depending on the particular placement, order of entry, and pairing of the different ions.

TABLE 1

Gibbs free energies and equilibrium dissociation constants for single- and double-ion occupancy from 2-D PMF computations

Occupancy group	Occupancy	Dissociation constant (mol/L)		ΔG (kcal/mol)
		K_D(single)	K_D(double)	ΔG
Single-ion occupancy	Na	4.88E-14		−19.19
	K	7.56E-12		−16.03
Na at innermost position	Na–Na		4.27E-03	−3.42
	K–Na		8.44E-03	−2.99
K at innermost position	K–K		9.85E-03	−2.89
	Na–K		7.29E-03	−3.08

Values were calculated from the following data: K_D (single) for Na, from Fig. 3 A, and from equivalent data for K; K_D (double) from the data in the 2-D PMFs in Fig. 3 C.

one-ion PMF, dissociation rates of $10^{-1} \sim 10^{-2}$ ions/s^{-1} are predicted from a single-barrier calculation based on Eyring rate theory. This is reminiscent of tight binding of Na^+ and Ca^{2+} to binding sites in model channels (Nonner and Eisenberg, 1998; Krauss et al., 2011). To reconcile large ionic fluxes, Krauss et al. (2011) argued for the existence of multiple binding sites and the importance of the local crowding effects. More realistic permeation pathways appear on the energy landscape when two monovalent cations enter into the pore (Fig. 3 C), with energy minima for four doubly occupied configurations in the range of −2 to −4 kcal/mole (Fig. 3, B and D). Then, low energy permeation pathways (blue tones) become clearly apparent; the potential profiles traversed by a single ion were obtained by integrating along the reaction coordinates (Fig. 3 D and see Materials and methods, Computational strategies). Similar findings have been reported recently from computational studies by Furini and Domene (2012) and by Corry and Thomas (2012). They also emphasize the need for a second bound ion to achieve physiological conductance levels. The relatively deep energy well for Na–Na would contribute to higher stability of Na–Na-occupied filter, with the essentially flat entrance barrier for Na–Na also playing a significant role (Z = 10 ∼ 12 Å) in discrimination among different ions. It is important to stress that uncertainties in 2-D PMF computations are rather high, but the resolution in the computed maps is still sufficient to clearly discriminate between Na–Na and K–K occupancy in the filter. Interestingly, in the case of K–K binding to the filter, there is a small barrier separating two ion-binding energy minima.

Extended analysis of the 2-D PMFs revealed multiple binding sites separated by small barriers (indicated in Fig. 3, C–E). The integrated single-ion PMFs (e.g., Fig. 3 D) and 1-D "cross-section" profiles (e.g., Fig. 3 E), derived from the 2-D PMF surfaces, help us to understand the significance of this apparent complexity in the filter. We estimated the corresponding equilibrium dissociation constants in the presence of constraints for the singly and doubly occupied channel using the following theoretical developments of Kim and Allen (2011) and Derebe et al. (2011). In general, the channel binds Na^+ in preference to K^+, but when two ions are bound, the magnitude of Na/K selectivity for binding at the first site depends on the identity of the second ion. With symmetric occupancy of the filter, binding of an Na^+–Na^+ pair is favored over a K^+–K^+ pair (Table 1). Up to three well-defined potential binding sites can be distinguished, further supporting the idea that multiple ions can occupy the pore. The free energy cost to bring in a third ion would render this occupancy unstable, thus leading to a permeation event. The effective free energy cost caused by ion–ion repulsion for bringing a second ion as determined from the single- and double-occupancy dissociation constants, K_s and K_d, is ∼13–16 kcal/mol depending on the cation species.

The mixed occupancies, Na–K and K–Na, yield intermediate depths, reflecting an effect on the stability of the binding around the middle of the selectivity filter. However, the PMF calculations are accurate only within ∼1 kcal/mol according to our block-average analysis placing restraints on the interpretation of obtained PMFs. Nevertheless, in the limits of method resolution, the barriers at the extracellular side of the channel display dependence on the combination of ions present, although the differences are subtle. In the case of the barriers, the mixed ion combinations provide the extremes, whereas double occupancy, by a single-ion species, Na–Na and K–K, yields the extremes. The number and the conformation of binding sites definitely differ considerably depending on the identity of the second ion. The free energy profile for Na^+, double occupancy (the solid black line in Fig. 3 D), has a local minimum of around Z = 3 Å, which is not present in the case of K^+ (the solid red line in Fig. 3 D). Also, binding sites around Z = 4.5 Å for Na^+ shifted to the right by ∼0.5 Å with respect to those for K^+.

"Selectivity" is asymmetric and shows a complex dependence on ionic composition of the solutions

Garber (1988) reported a striking asymmetry of reversal potentials for skeletal muscle Nav channels in planar lipid bilayers, measured when a bi-ionic Na/K gradient was

reversed. Similar behavior has also been reported recently by a mutant version of nonselective NaK channel by Derebe et al. (2011).

We observed an analogous result for NaChBac whole-cell currents, when K^+_{ext} was exchanged for Na^+_{ext} in the presence of either internal Na^+ or K^+ (Fig. 4 C). The magnitude of the reversal potential shift, after external ion replacement, was ∼100 mV with internal Na^+ but only ∼40 mV with internal K^+, yielding a 10-fold difference in P_K/P_{Na} calculated with oppositely directed gradients (P_K/P_{Na} = 0.2 with internal K^+, and 0.02 with internal Na^+). In bi-ionic conditions, with isotonic Na^+ and K^+ solutions on opposite sides of the membrane, the reversal potentials were approximately +45 mV (Na^+ inside) and −100 mV (Na^+ out; instantaneous I-V relations; data points plotted as open triangles; see Fig. 4 C). This functional asymmetry may reflect a common property among the various members of the P-loop family of channels, which possess a nonselective entrance to the intracellular cavity, and a selectivity filter located nearer to the extracellular mouth.

In doing these experiments, we also noted a kinetic asymmetry. The approach to a new steady-state level of peak currents elicited by a succession of identical voltage-clamp pulses took significantly longer for washout of external K^+ by Na^+ than vice versa (Fig. 4, A and B), suggesting stronger binding of K^+ within the pore. This difference was most obvious with Na^+ as the only internal cation species, but it was also significant with K^+ as the only intracellular cation. Slow washout of potassium was also seen with cesium as the only internal cation, but it was not detectable using mixtures of cesium or potassium with sodium (Fig. S1, A–D).

Dependence of conductance on extracellular mole fraction in sodium–potassium mixtures

Progressive substitution of external Na^+ by K^+ reveals a nonmonotonic (anomalous) dependence of conductance

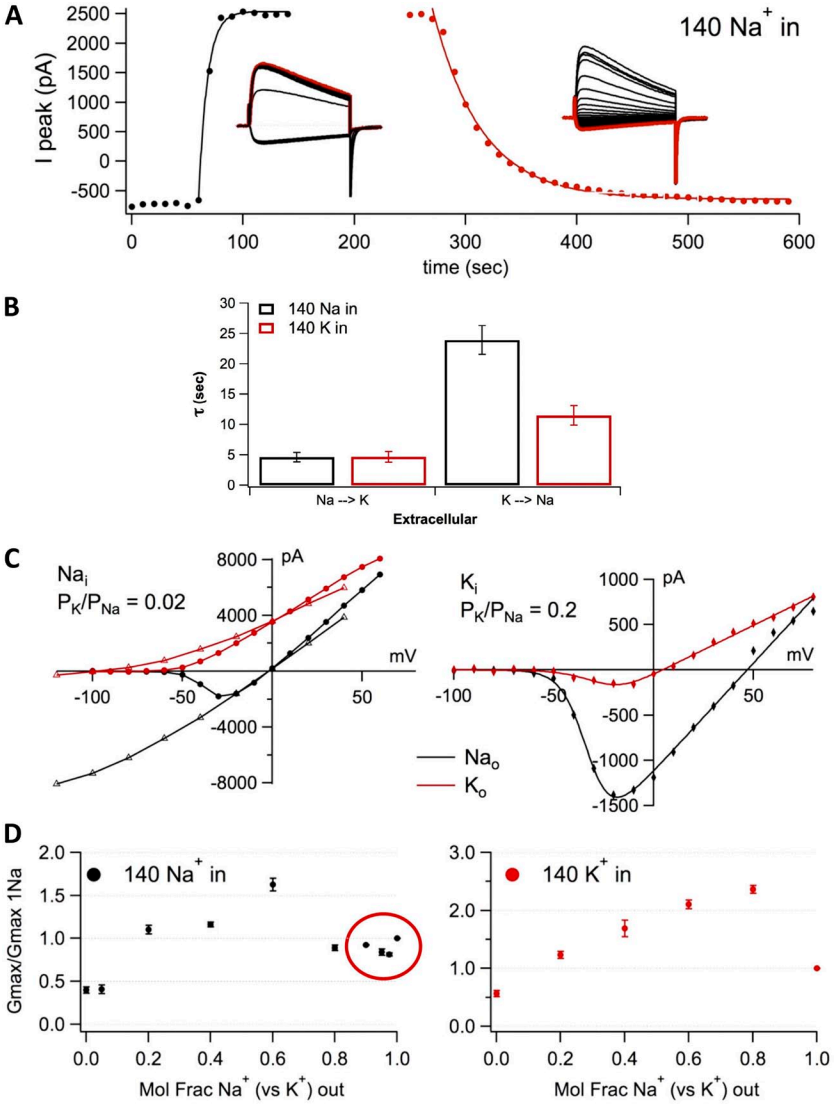

Figure 4. K^+ binding in the pore, asymmetry of bi-ionic Na–K reversal potentials, and anomalous mole-fraction dependence of conductance. (A) Representative wash-in and washout time courses, observed when a 142.5-mM Na^+ extracellular solution is fully replaced by 142.5 mM K^+, and is subsequently washed out. Insets show current traces in response to a −10-mV stimulation every 10 s with $[Na^+]_i$ = 140 mM. (B) Time constants derived from exponential fits to the wash-in (Na→K) and washout (K→Na) for four different intracellular solutions. Internal alkali cation concentrations were (mM): 35 Na (35 Na and 105 Cs), 35 K (35 K and 105 Cs), 140 Na (140 Na), and 140 K (140 K). (C) I-V relationships indicating bi-ionic reversal potentials determined for K_o/Na_i (left) and Na_o/K_i (right). The reversal potentials change asymmetrically when the ionic gradients are reversed in direction. Note that clear measurement of reversal potentials for the bi-ionic case internal sodium/external potassium required instantaneous I-V data (left, open triangles; see Materials and methods, Data analysis, for more details). In all other cases, reversal potentials were determined from peak I-V relations. (D) Maximal conductance, Gmax, normalized with respect to the control value in full sodium external solution (f_{Na} = 1), plotted against the extracellular mole fraction of Na (f_{Na}). Prominent maxima are seen at intermediate values of f_{Na} for both internal Na and internal K, and a small but significant local minimum (circled) appears, for internal Na only, near f_{Na} = 1. Note that error bars (±SEM) are plotted on all points. See text for further details.

on mole fraction of sodium, f_{Na} (Fig. 4 D). Such behavior has frequently been associated with multi-ion occupancy of channels and repulsive interactions among ions in the channel, although alternate explanations have been proposed. The following features are of interest in our data. With a single monovalent cation species inside—either sodium or potassium—there is a general tendency for conductance to increase in a supra-linear fashion up to f_{Na} = 0.6. With potassium as the sole internal cation species, a conductance maximum occurs at $f_{Na} \approx 0.8$, and the conductance then declines monotonically to the value characteristic of a full sodium external solution. Notably, the appearance of this maximum appears specific to interactions between Na^+ and K^+, as we saw no maximum with internal solutions containing 105 mM Cs^+, plus 35 mM of either Na^+ or K^+ (see Fig. S1, E and F). If the sole internal cation species is sodium, a shallow local minimum also appears in the conductance at $f_{Na} \approx 0.95$ (Fig. 4 D). This result provides further evidence that the last K^+ ion to exit binds tightly enough to make it relatively difficult to completely wash potassium ions out of the channel (see also Fig. 4 A), consistent with the tight binding predicted by 1-D PMFs.

Two features of these data deserve attention. First, the maxima we see for intermediate mole fractions (f_{Na} = 0.6–0.8) are unusual, and to our knowledge have not been reported previously for other systems. Thus, the conductance is higher for external mixtures of Na and K than with either Na or K as the sole external species. This would be consistent with an evolutionary optimization for conduction in physiological solutions containing mixtures of sodium and potassium.

In other reported cases of an anomalous mole-fraction effect involving K or Cav channels, a minimum in mole-fraction dependence has been seen, suggesting that one ion species binds strongly enough to impede permeation by another (Hille and Schwarz, 1978; Hess and Tsien, 1984; Eisenman et al., 1986). A similar mechanism may underlie the local minimum that we show in Fig. 4 D, at $f_{Na} \approx 0.95$, with Na^+ as the internal monovalent cation species.

Simulating ion–ion interactions

To explore the role of a particular bound ion on the entrance barriers for the second ion, we used a cross-section methodology from Li et al. (2010) applied to a bi-ionic solution, where a 1-D PMF ("cross section") for a permeating ion, in the presence of a fixed copermeant ion, was obtained from a 2-D map (Fig. 3 E). The bound ion was fixed at Z = 1.0 Å. As expected, the barriers presented near the entrance (Z > 12 Å) display relatively little dependence on a particular combination of

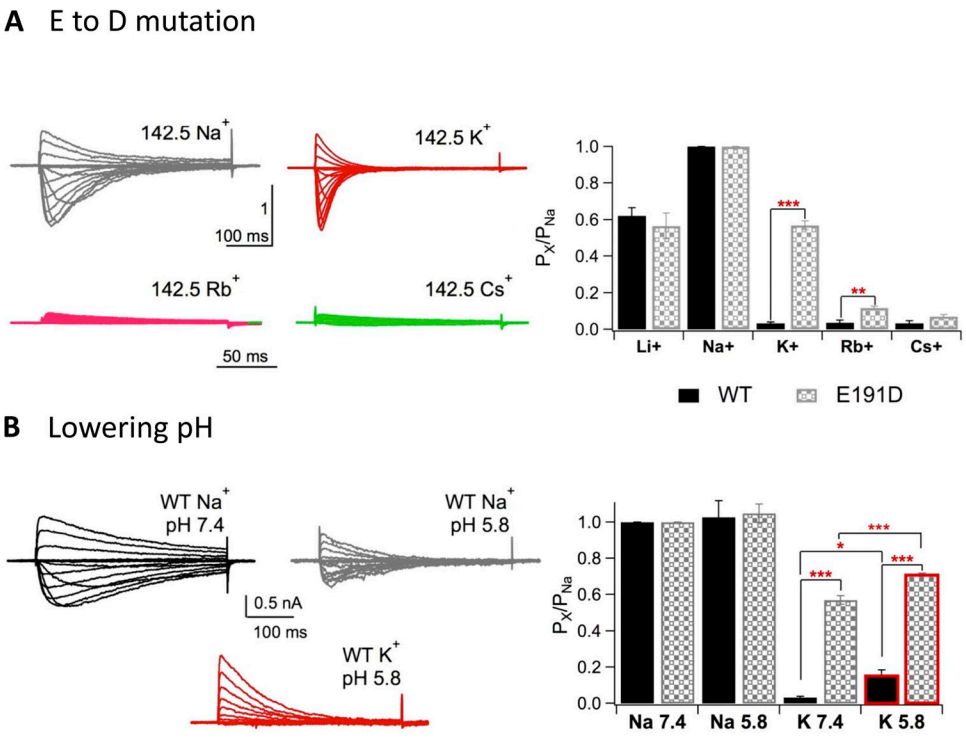

Figure 5. Roles of side-chain length and negative charge density in the selectivity filter. Both experimental manipulations (E191D substitution and lowering of the external pH) reduce selectivity among alkali cations. (A) Representative E191D mutant–mediated currents in the presence of different extracellular alkali cations at pH 7.4. The bar graph on the right shows significant increases in both P_K/PNa and P_{Rb}/P_{Na} after the E191D substitution. (B) NaChBac WT current traces recorded in the presence of Na and K at pH 5.8. To better resolve reversal potentials for external K, they were determined from instantaneous I-V relations after a depolarizing prepulse used to maximally activate the channels (see Materials and methods, and Fig. 4). Permeability ratios for WT and E191D mutant channels at neutral and acid pH are summarized in the bar graph on the right. Discrimination between Na^+ and K^+ is reduced at pH 5.8 for both NaChBac WT and for the E191D mutant. Probabilities, P, for different comparisons are indicated as follows: *, <0.05; **, <0.01; ***, <0.0001.

cations. Within the selectivity filter (Z = 4–8 Å), the situation is drastically different among the Na–Na, Na–K K–Na, and K–K combinations. The interaction between cations in the filter can significantly affect the relative height of the barrier and the depth of the well experienced by a second cation. The ion bound to the lowest affinity site (Z = 1.0 Å) also affects the location of the binding site for the entering cation. Notably, K–Na mixtures tend to display flatter energy profiles, suggesting that the conductance for a mixture of cations could be as high as for pure Na^+ solution based on reduction of the entrance barrier for the second cation.

It is important to stress some limitations of our present analysis. It is based on a crystal structure for closed state, where complete integration of the permeation profile is impossible. Estimates of the mutual repulsion among permeant ions, and corresponding pore–ion interactions, would also depend on the force field used to analyze them.

Permeation volume of the selectivity filter and discrimination among alkali cations

Discrimination among alkali cations by NaChBac is qualitatively similar to that shown by eukaryotic Nav channels (Hille, 1972). For NaChBac, under the conditions of our experiments (single monovalent cation species, X, in the extracellular solution, with an intracellular solution containing 35 mM Na and 105 mM Cs), the relative permeabilities, P_X/P_{Na}, fall into the following sequence: Li ≈ Na > K ≈ Rb ≈ Cs. Given the difference in net charge on the selectivity rings between bacterial (EEEE) and eukaryotic sodium channels (DEKA), an obvious question arises: how do changes in the net charge on the selectivity filter affect selectivity?

Replacement of the selectivity filter glutamate with aspartate (E191D in NaChBac and E177D in NavAb) would yield a DDDD selectivity ring. With minimal perturbation in the backbone structure, this substitution might have been expected to lead to a small increase in diameter, with a consequent reduction in negative charge density at the selectivity filter, and because of the shorter aspartate side chains. Actually, the energy-minimized structure for E177D shows a slightly reduced diameter because of the more direct projection of the side chain toward the pore axis than for the longer, more flexible glutamate (Figs. 1 B and 6 A). The resultant decrease in radius is associated with the removal of the multiple energy minima seen in 2-D PMFs, and it yields almost indistinguishable single-ion PMFs for Na^+ and K^+ (Fig. 6 D).

Experimentally, this mutant showed a decrease in selectivity for Na^+, with significant increases in relative permeability to both potassium and rubidium compared with the WT channel (Fig. 5 A). In a complementary set of experiments, lowering the extracellular pH from 7.4 to 5.8, which is expected to titrate some of the charge on the EEEE selectivity ring, reduced the discrimination among alkali cations (Figs. 5 B and S3). For both WT NaChBac and the mutant E191D, the lowered external pH yielded an increased relative permeability to potassium. The permeability increase was slightly larger for the E191D mutant, such that this construct did not distinguish between extracellular Na^+ and K^+ at pH 5.8. Collectively, the experiments in this section suggest that charge density within the selectivity ring is an important contributor to overall selectivity among the alkali cations.

To test whether the pore cross section is affected by E191D replacement, we ran a complementary set of all-atom MD simulations on a mutated pore. The calculated cross-sectional profiles for NavAb E177D are shown in Fig. 6 A. The pore radius at the constriction is still considerably wider than that for K channels. This finding is in keeping with previous data on the ion hydration in the pore (Corry and Thomas, 2012; Treptow and Klein, 2012), which suggest that the permeant cation (either Na^+ or K^+) is able to maintain partial hydration and could possibly be accommodated by either WT or E/D mutant. The pore radius decreased slightly with the E177D mutation despite the shorter side chain introduced. To further investigate the mechanisms by which the E/D mutation might reduce selectivity, we again used a 2-D PMF-based strategy similar to that in the WT sections. The resulting 2-D PMFs for Na^+/Na^+ and K^+/K^+ are shown in Fig. 6 C, and the corresponding single-ion PMFs are shown in Fig. 6 B. The PMF calculations show considerable changes in the energy surface, which controls ion transport across NavAb E177D. The computations suggest that the degree of ion stabilization in two of the three proposed binding sites present in the WT filter (Fig. 1 A) is significantly affected by the mutation. The first binding site (S_{HFS}) is destabilized for both Na^+ and K^+ (Fig. 6 B), whereas the second binding site (S_{IN}) remains virtually unaffected. It is tempting to think that E/D mutation not only affects the cross section of the pore but also ion coordination environment and number of sites available to an ion along the permeation pathway. The significant destabilization of one of the ion-binding sites caused by mutation would reduce the likelihood of two ions binding simultaneously to the filter.

The computed PMFs suggest that the differences in Na/K profiles, present in WT, are largely gone when this mutation is present, and it is also evident that there are several significant rearrangements in the ion coordination in the filter region. The entrance binding site, *ii*, presented in the WT (Fig. 3 C) is eliminated in the mutant for both Na^+ and K^+ binding to E/D–NavAb, whereas central binding sites (*iii* and *iv*) display similar stability for Na^+ and K^+. This finding is in agreement with our experimental data on ion selectivity (Fig. 5 A). Thus, the reduced selectivity of the E-D mutant may be primarily attributed to the removal of one of the binding sites from the selectivity filter coupled with a nondiscriminatory

binding of Na^+ and K^+ to the remaining site (Fig. 6, B and C). These results highlight an importance of the multiple binding sites present in the selectivity filter, which appears to modulate selective conductance.

DISCUSSION

Overview: Defining selectivity

A definition of the "selectivity" of an ion channel could be based on measurements of ion-binding affinity, conductance, or reversal potential for currents measured under particular conditions. Under fairly general conditions (Patlak, 1960), "relative permeabilities" thus calculated (see Materials and methods) directly reflect the rate of unidirectional flux across the membrane (Goldman, 1943; Hodgkin et al., 1952), or the rate of entry into the channel (Hille, 1975a). Although this simple physical interpretation likely breaks down with complex barrier profiles or ion–ion interactions (Eisenman and Horn, 1983), relative permeability provides a widely used method to establish selectivity sequences among the various ions that can pass through a channel.

In the following discussion, we establish selectivity sequences among the alkali cations for NaChBac and its point mutant, E191D, at both normal and acidic pH. We go on to examine the complex concentration dependence of conductance to gain insight into ion binding to the channel and intrapore ion–ion interactions among ions within the pore. In the context of these experimental results, we use MD and free energy calculations based on the structure of NavAb, a close relative of NaChBac.

Summary of experimental results

Homotetrameric NaChBac, despite its more symmetric structure, qualitatively resembles eukaryotic Nav channels in that it selectively conducts Na in preference to most other monovalent ions and common physiological divalents. The selectivity "fingerprint," defined as the order of relative permeabilities, P_X/P_{Na}, for the alkali cations is indistinguishable from that seen for eukaryotic channels: Li ≈ Na > K ≈ Rb ≈ Cs (Fig. 2 C). As suggested

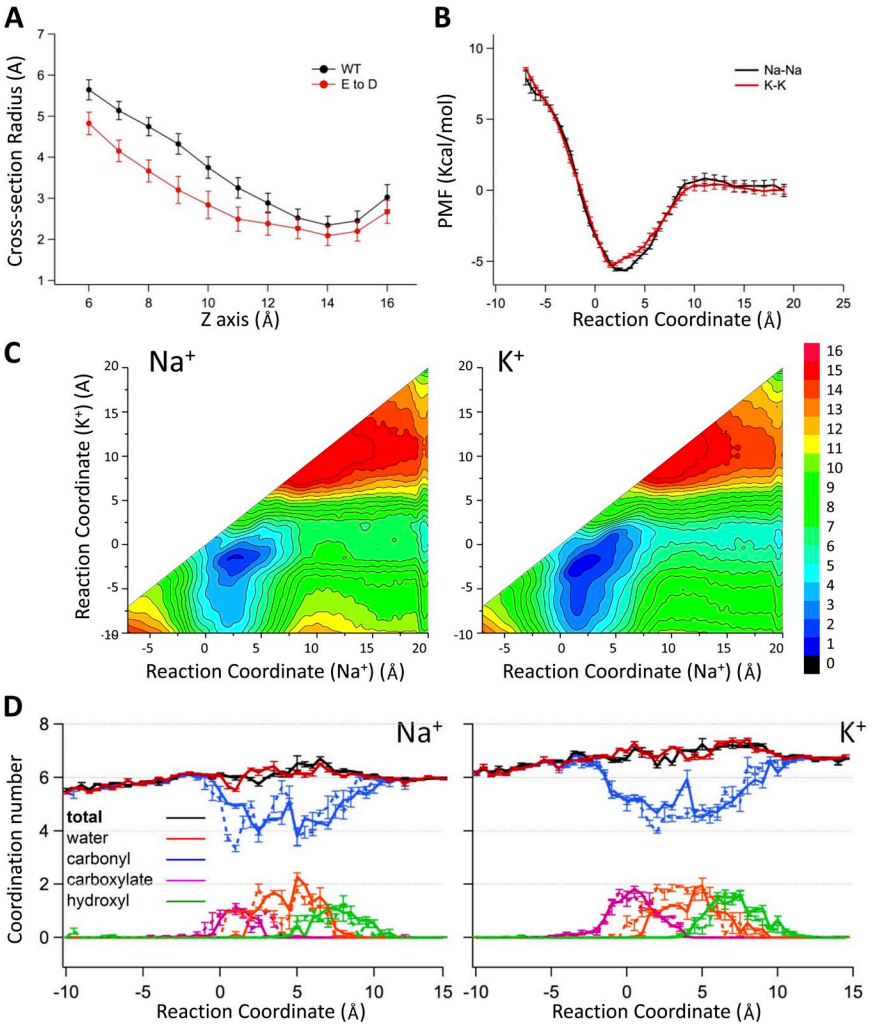

Figure 6. Predicted consequences of a charge-conserving selectivity filter mutation (NavAb E177D). (A) Compared with NavAb WT, there is a decrease in radius of the cylindrical cross section available for ion permeation along the pore axis for the E177D mutant. (B) 1-D PMFs integrated from 2-D PMF maps (c.f., Fig. 3 D) from C for Na^+ and K^+ transport through NavAb E177D. The lower entry barrier for K^+ would favor a higher value of P_K/P_{Na}, thus lowering selectivity, as experimentally observed for NaChBac E191D. (C) Contour plots of 2-D PMFs, which provide the 1-D plots in D, for occupancies by Na^+/Na^+ and K^+/K^+ in the NavAb E177D selectivity filter. (D) Average coordination numbers for sodium or potassium ions at different ion positions in the transport process for NavAb WT and for E177D are shown as solid and dotted lines, respectively (for coordination group identity, see the color key in the figure). Coordination numbers represent the mean numbers of oxygen atoms, which are found within 3.5 Å of an ion, as water, carbonyl, carboxylate, or hydroxyl groups. The choice of the unique confinement radius is a challenging issue. We based our choice for the size of the coordination shell on an analysis that was chosen in accordance with our previous studies on ion hydration by aqueous clusters and model protein sites (Yu et al., 2010; Lev et al., 2013), where it was found to faithfully reproduce relative free energies. In addition, the total number of coordinating oxygen atoms is shown by the solid red and black lines.

by earlier work (Ren et al., 2001), the critical physiological selection for Na over K appears to be somewhat more stringent for NaChBac than for eukaryotic channels (NaChBac, $P_K/P_{Na} = 0.03 \pm 0.007(4)$ compared with 0.048–0.086 for four eukaryotic Nav channel variants; see Table 14.2 in Hille, 2001).

A functional asymmetry, common to NaChBac and eukaryotic channels, is seen in the inequality of magnitude of reversal potentials observed when a bi-ionic Na/K gradient is reversed. Reversal potentials of approximately −100 mV (Na_i/K_o) and approximately +40 mV (K_i/Na_o) indicate a 10-fold stronger discrimination between K and Na when the internal cation species is Na than for the reverse case (Fig. 4 C). Alkaloid-modified rat muscle Nav channels (bound by a large alkaloid, batrachotoxin or veratridine, in the cytoplasmic cavity) show many of the qualitative properties of unmodified channels, including an asymmetry of bi-ionic reversal potentials (Garber, 1988). This suggests that important determinants of selectivity reside near the outer end of the pore. The results also indicate the usefulness of a "pre-open" structure as a relevant basis for simulations of selectivity, particularly discrimination among extracellular ions, even though the intracellular bundle-crossing gate may be closed or modified.

The dependence on external mole fraction in bi-ionic Na–K mixtures ($f_{Na} = [Na]_o/([Na]_o + [K]_o)$) of the normalized maximal conductance is highly nonmonotonic (Fig. 4 D). A clear maximum appears at intermediate values of f_{Na} (0.6–0.8), suggesting that mixed occupancy by Na and K, as would be expected under physiological conditions, enhances conductance. In addition, a less conspicuous but significant local minimum, which occurs at low levels of K_o ($f_{Na} \approx 0.95$–0.97), hints that a single potassium ion binding at the outer end of the pore may inhibit sodium permeation. Anomalous (nonlinear and nonmonotonic) mole-fraction dependence has generally been associated with multi-occupancy with ion–ion interactions in the pore. This is consistent with our own calculations (Fig. 3) and those of others (Yue and Marban, 1990), but alternate explanations have been proposed (Nonner et al., 1998; Gillespie and Boda, 2008). NaChBac's strong anomalous mole-fraction dependence, with its distinctive enhancement of conductance at intermediate mole fractions, was observed only with intracellular solutions containing solely Na, or solely K, as cations.

Two maneuvers, which might be expected to change the charge density on the selectivity filter (E191D mutation and lowering of pH), each reduce NaChBac's ability to discriminate between Na and K (Fig. 5), as predicted by Corry and Thomas (2012). Accordingly, our data show that lowering pH from 7.4 to 5.8 increases P_K/P_{Na} significantly from $0.03 \pm 0.006(4)$ to $0.15 \pm 0.03(6)$ ($P = 0.018$; see Fig. 5 B).

The E191D substitution also reduces selectivity, with $P_K/P_{Na} = 0.57 \pm 0.02(4)$ at pH 7.4 and a further increase to $0.71 \pm 0.01(4)$ at pH 5.8. It is not intuitively obvious why the decrease in pore diameter (Fig. 6 A) should be associated with a decrease in selectivity, but at least it does suggest that energetic factors beyond simple steric filtering, or simple binding interactions dependent on the field strength near a coordinating site, must be considered to account for this change, together with the other complexities of the dataset.

Computational studies

Insight from atomistic simulations is essential to study the mechanism of ion permeation through NavAb channels. Without such a quantitative approach, coordinated with experimental studies, the binding sites proposed based on the crystal structure would remain speculative. The deep energy wells shown in 1-D PMF profiles (e.g., Fig. 3 A) indicate that single Na^+ or K^+ ions are extremely unlikely to permeate though the channel. Calculations based on 2-D PMFs provide more realistic permeation pathways, with energy minima in the range of −2 to −4 kcal/mol (Fig. 3, B and D). The blue tones in the energy landscapes show many stable conformations and multiple favorable ion-binding sites.

All three binding sites, which were previously hypothesized based on the structure (Payandeh et al., 2011), are consistent with our simulations. In the 2-D PMF maps, S_{IN} appears in the stable conformations but not necessarily S_{CEN}. The outer binding site S_{HFS} is not stable because of the flexibility of the Glu177 side chains, but Glu 177 can form a binding site with the help of the side chain oxygen atom of Ser178. It can also contribute to the coordination shell of a Na^+ ion, together with the Leu176 side chain of the neighboring monomer in S_{CEN}. Finally, it can even form a binding site in partnership with Leu176 of the same chain. The computational results also indicate that the ion does not move along the central pore axis (Fig. 3 C) because of the relatively large radius of the channel (Fig. 6 A). Instead, an ion is coordinated by the main chains and charged side chains from one or two of the monomers, and by water molecules (Figs. 3, A and C, and 6 E). In addition, MD simulations with different ion configurations inside the channel pore suggest that movement of the ions is weakly coupled compared with the strong coupling in K^+ channels, which provide a very snug fit for their preferred ion species.

The most important biological function of Na^+ channels is to catalyze Na^+ permeation into the cell, while simultaneously preventing permeation by K^+ ions. Within the integrated 2-D PMFs (Fig. 3 D), the barriers and wells depend on the occupancy in the filter. Na–Na displays the deepest energy wells, whereas K–K has the shallowest ones in the filter, indicating that the channel selectively binds Na^+. Calculation of the free energy of binding for two ions indicates that binding of the ion pair, Na–Na, is favored over K–K (Table 1). Furthermore, an entering Na^+ ion needs to overcome a relatively high energy

barrier to reach the energy minimum in the selectivity filter, when a K^+ is already present (panel Na–K). This is further illustrated in the 1-D cross sections (Fig. 3 E), where one ion, K^+, is fixed in the filter at the position corresponding to the stable minimum. This example shows that it is energetically feasible for Na^+ to pass K^+ in the narrowest part of the filter, even though this may not represent the most probable reaction pathway for permeation.

Comparison of the 2-D PMFs for E177D (Fig. 6 C) shows that this mutation decreased the number of potential binding sites (Fig. 6 D). Furthermore, this conservative amino-acid substitution modulates the relative numbers of different coordinating ligands, thus altering local chemical moieties involved in ion coordination leading nearly the same relative binding free energies for Na^+ and K^+ to the filter. To illustrate how ion coordination along the permeation pathway is affected by the mutation, we performed analysis of the position-dependent ion coordination sphere for stable binding sites found in 2-D PMF maps (Fig. 6 D). The average coordination number of Na^+ and K^+ does not change substantially with the E/D mutation. However, the chemical composition of the coordination sphere does. There is a small decrease in the average number of carboxylates coordinating each Na^+ ion from the extracellular side to the position of Z = 2.5 Å (free energy minimum for Na^+), as shown in Table 2. Meanwhile, the probability of finding carboxylates in the potassium coordination sphere increases by ∼60% in both stable sites identified by the PMF computations. Therefore, in the mutant, K^+ can gain additional stabilization from carboxylates, whereas this mode of K^+ coordination is largely missing in the WT. At the same time, K^+ coordination by water decreases as compared with the WT protein. The water ligating K^+ in the WT is replaced by carboxylates in the mutated pore. For example, in NaVAb E177D, the coordination with carboxyl oxygens was substituted by coordination with water molecules for Na^+ but not for K^+ (Fig. 6 D). Therefore, hydration and coordination in the pore combine to play an important role, which appears sufficient to define the properties of an important ion-binding site and the entry barrier of bacterial Nav channels. The results of PMF computations together with coordination analysis are consistent with the experimentally observed increase in relative potassium permeability. Thus, the E/D mutation allows for more favorable K^+ binding to the filter as compared with WT. There are, of course, limitations imposed on our analysis by the use of a closed or "pre-open" structure to explore the underpinnings of selectivity. Certainly, a prediction of absolute ion throughput and conductance will require detailed analysis of an open pore structure, preferably for a channel from which single-channel data can be obtained. However, by focusing our analysis on experiments evaluating selectivity based on ion interactions near the extracellular entrance, we believe that we have obtained significant insight into the physiologically crucial discrimination between Na^+ and K^+ by these channels.

TABLE 2

Site-dependent ion coordination probabilities for NavAb WT and E177D

Position of the binding site	COO—Coordination probability			
Z (Å)	WT-SOD	E/D-SOD	WT-POT	E/D-POT
3.0	0.38	0.25	0.29	0.47
2.5	0.27	0.46	0.28	0.41

Entries represent the probabilities of finding carboxylate in the coordination sphere of an ion. P = 1 corresponds to all four selectivity filter carboxylates engaged in ion coordination. See also Fig. 6 D and its legend.

Concluding comments

The key strategy adopted by prokaryotic Nav channels to discriminate against K^+ is as follows. First, the pore is large enough to allow for permeation of variably hydrated cations. Second, within the selectivity filter, ion coordination is highly dynamic, and a fine balance among ion ligation from carboxylates, carbonyls, and water molecules is at the heart of the selective entry and occupancy by external ions. Third, although a single binding site inside the filter displays a preference for Na^+ over K^+, two-ion states are thermodynamically stable and are essential for rapid permeation. Finally, two procedures likely to modify the charge density near the narrowest point in the selectivity filter (E-D substitution and reduction of pH) reduce the discrimination between Na^+ and K^+, likely because of small changes of both energy minima and maxima in the PMFs for the two ions.

Our results are consistent with a scenario in which differing selective pressures, during the evolution of prokaryotes and eukaryotes, favored a common need for sodium selectivity. However, each phylogenetic lineage would presumably have been subject to differing selection for other properties, such as details of channel gating kinetics, the necessity to function in different ionic conditions, and the presence of other complementary ion channels. Ultimately, the various, sometimes conflicting, evolutionary demands on overlapping components of channel structure appear to have yielded different but almost equally effective "choices" of the molecular strategy to generate a sodium-selective conductance in prokaryotes compared with eukaryotes.

We are grateful to Drs. Harry Fozzard, Richard Horn, Eduardo Perozo, and Peter Tieleman, for reading a draft of the manuscript. We thank Drs. Paul DeCaen and David Clapham for sharing unpublished data and for helpful discussions.

This work was supported by operating funds from: Canadian Institutes of Health Research Grants MOP-10053 (to R.J. French and R.K. Finol-Urdaneta) and MOP-186232 (to S.Y. Noskov and Y. Wang); the National Science and Engineering Research Council Discovery Grants RGPIN/418658-2012 (to R.J. French and R.K.

Finol-Urdaneta) and RGPIN 340946-07 (to S.Y. Noskov and C. Zhao); and the Heart and Stroke Foundation of Alberta and Northwest Territories (to S.Y. Noskov and Y. Wang). S.Y. Noskov is an Alberta Innovates Health Research Scholar. Preliminary experiments were performed by Jeff McArthur and Eva Ouyang.

The authors have no conflicting financial interests.

Lawrence G. Palmer served as editor.

Submitted: 24 May 2013
Accepted: 23 December 2013

REFERENCES

Adams, D.J., T.M. Dwyer, and B. Hille. 1980. The permeability of endplate channels to monovalent and divalent metal cations. *J. Gen. Physiol.* 75:493–510. http://dx.doi.org/10.1085/jgp.75.5.493

Allen, T.W., O.S. Andersen, and B. Roux. 2004. Energetics of ion conduction through the gramicidin channel. *Proc. Natl. Acad. Sci. USA.* 101:117–122. http://dx.doi.org/10.1073/pnas.2635314100

Backx, P.H., D.T. Yue, J.H. Lawrence, E. Marban, and G.F. Tomaselli. 1992. Molecular localization of an ion-binding site within the pore of mammalian sodium channels. *Science.* 257:248–251. http://dx.doi.org/10.1126/science.1321496

Bezanilla, F., and C.M. Armstrong. 1972. Negative conductance caused by entry of sodium and cesium ions into the potassium channels of squid axons. *J. Gen. Physiol.* 60:588–608. http://dx.doi.org/10.1085/jgp.60.5.588

Brooks, B.R., C.L. Brooks III, A.D. Mackerell Jr., L. Nilsson, R.J. Petrella, B. Roux, Y. Won, G. Archontis, C. Bartels, S. Boresch, et al. 2009. CHARMM: the biomolecular simulation program. *J. Comput. Chem.* 30:1545–1614. http://dx.doi.org/10.1002/jcc.21287

Busath, D., and T. Begenisich. 1982. Unidirectional sodium and potassium fluxes through the sodium channel of squid giant axons. *Biophys. J.* 40:41–49. http://dx.doi.org/10.1016/S0006-3495(82)84456-1

Corry, B., and M. Thomas. 2012. Mechanism of ion permeation and selectivity in a voltage gated sodium channel. *J. Am. Chem. Soc.* 134:1840–1846. http://dx.doi.org/10.1021/ja210020h

Derebe, M.G., D.B. Sauer, W. Zeng, A. Alam, N. Shi, and Y. Jiang. 2011. Tuning the ion selectivity of tetrameric cation channels by changing the number of ion binding sites. *Proc. Natl. Acad. Sci. USA.* 108:598–602. http://dx.doi.org/10.1073/pnas.1013636108

Doyle, D.A., J. Morais Cabral, R.A. Pfuetzner, A. Kuo, J.M. Gulbis, S.L. Cohen, B.T. Chait, and R. MacKinnon. 1998. The structure of the potassium channel: molecular basis of K^+ conduction and selectivity. *Science.* 280:69–77. http://dx.doi.org/10.1126/science.280.5360.69

Eisenman, G. 1962. Cation selective glass electrodes and their mode of operation. *Biophys. J.* 2:259–323. http://dx.doi.org/10.1016/S0006-3495(62)86959-8

Eisenman, G., and R. Horn. 1983. Ionic selectivity revisited: the role of kinetic and equilibrium processes in ion permeation through channels. *J. Membr. Biol.* 76:197–225. http://dx.doi.org/10.1007/BF01870364

Eisenman, G., R. Latorre, and C. Miller. 1986. Multi-ion conduction and selectivity in the high-conductance Ca++-activated K+ channel from skeletal muscle. *Biophys. J.* 50:1025–1034. http://dx.doi.org/10.1016/S0006-3495(86)83546-9

Essmann, U., L. Perera, M.L. Berkowitz, T. Darden, H. Lee, and L.G. Pedersen. 1995. A smooth particle mesh Ewald method. *J. Chem. Phys.* 103:8577–8593. http://dx.doi.org/10.1063/1.470117

Feller, S.E., and A.D. MacKerell. 2000. An improved empirical potential energy function for molecular simulations of phospholipids. *J. Phys. Chem. B.* 104:7510–7515.

French, R.J., J.F. Worley III, W.F. Wonderlin, A.S. Kularatna, and B.K. Krueger. 1994. Ion permeation, divalent ion block, and chemical modification of single sodium channels. Description by single- and double-occupancy rate-theory models. *J. Gen. Physiol.* 103:447–470. http://dx.doi.org/10.1085/jgp.103.3.447

Furini, S., and C. Domene. 2012. On conduction in a bacterial sodium channel. *PLOS Comput. Biol.* 8:e1002476. http://dx.doi.org/10.1371/journal.pcbi.1002476

Garber, S.S. 1988. Symmetry and asymmetry of permeation through toxin-modified Na^+ channels. *Biophys. J.* 54:767–776. http://dx.doi.org/10.1016/S0006-3495(88)83014-5

Gillespie, D., and D. Boda. 2008. The anomalous mole fraction effect in calcium channels: a measure of preferential selectivity. *Biophys. J.* 95:2658–2672. http://dx.doi.org/10.1529/biophysj.107.127977

Goldman, D.E. 1943. Potential, impedance, and rectification in membranes. *J. Gen. Physiol.* 27:37–60. http://dx.doi.org/10.1085/jgp.27.1.37

Grossfield, A. 2012. WHAM: the weighted histogram analysis method. Version 2.0.6. http://membrane.urmc.rochester.edu/content/wham (accessed December 27, 2013).

Heginbotham, L., Z. Lu, T. Abramson, and R. MacKinnon. 1994. Mutations in the K^+ channel signature sequence. *Biophys. J.* 66:1061–1067. http://dx.doi.org/10.1016/S0006-3495(94)80887-2

Heinemann, S.H., H. Terlau, W. Stühmer, K. Imoto, and S. Numa. 1992. Calcium channel characteristics conferred on the sodium channel by single mutations. *Nature.* 356:441–443. http://dx.doi.org/10.1038/356441a0

Hess, P., and R.W. Tsien. 1984. Mechanism of ion permeation through calcium channels. *Nature.* 309:453–456. http://dx.doi.org/10.1038/309453a0

Hille, B. 1971. The permeability of the sodium channel to organic cations in myelinated nerve. *J. Gen. Physiol.* 58:599–619. http://dx.doi.org/10.1085/jgp.58.6.599

Hille, B. 1972. The permeability of the sodium channel to metal cations in myelinated nerve. *J. Gen. Physiol.* 59:637–658. http://dx.doi.org/10.1085/jgp.59.6.637

Hille, B. 1973. Potassium channels in myelinated nerve. Selective permeability to small cations. *J. Gen. Physiol.* 61:669–686. http://dx.doi.org/10.1085/jgp.61.6.669

Hille, B. 1975a. Ionic selectivity of Na and K channels of nerve membranes. *Membranes.* 3:255–323.

Hille, B. 1975b. Ionic selectivity, saturation, and block in sodium channels. A four-barrier model. *J. Gen. Physiol.* 66:535–560. http://dx.doi.org/10.1085/jgp.66.5.535

Hille, B. 2001. Ion channels of Excitable Membranes. Third edition. Sinauer Associates, Sunderland, MA. 814 pp.

Hille, B., and W. Schwarz. 1978. Potassium channels as multi-ion single-file pores. *J. Gen. Physiol.* 72:409–442. http://dx.doi.org/10.1085/jgp.72.4.409

Hodgkin, A.L., and R.D. Keynes. 1955. The potassium permeability of a giant nerve fibre. *J. Physiol.* 128:61–88.

Hodgkin, A.L., A.F. Huxley, and B. Katz. 1952. Measurement of current-voltage relations in the membrane of the giant axon of Loligo. *J. Physiol.* 116:424–448.

Jo, S., T. Kim, V.G. Iyer, and W. Im. 2008. CHARMM-GUI: a web-based graphical user interface for CHARMM. *J. Comput. Chem.* 29:1859–1865. http://dx.doi.org/10.1002/jcc.20945

Khan, A., L. Romantseva, A. Lam, G. Lipkind, and H.A. Fozzard. 2002. Role of outer ring carboxylates of the rat skeletal muscle sodium channel pore in proton block. *J. Physiol.* 543:71–84. http://dx.doi.org/10.1113/jphysiol.2002.021014

Kim, I., and T.W. Allen. 2011. On the selective ion binding hypothesis for potassium channels. *Proc. Natl. Acad. Sci. USA.* 108:17963–17968. http://dx.doi.org/10.1073/pnas.1110735108

Kim, M.S., T. Morii, L.X. Sun, K. Imoto, and Y. Mori. 1993. Structural determinants of ion selectivity in brain calcium channel. *FEBS Lett.* 318:145–148. http://dx.doi.org/10.1016/0014-5793(93)80009-J

Krauss, D., B. Eisenberg, and D. Gillespie. 2011. Selectivity sequences in a model calcium channel: role of electrostatic field strength. *Eur. Biophys. J.* 40:775–782. http://dx.doi.org/10.1007/s00249-011-0691-6

Kumar, S., D. Bouzida, R.H. Swendsen, P.A. Kollman, and J.M. Rosenberg. 1992. THE weighted histogram analysis method for free-energy calculations on biomolecules. I. The method. *J. Comput. Chem.* 13:1011–1021. http://dx.doi.org/10.1002/jcc.540130812

Lev, B., B. Roux, and S.Y. Noskov. 2013. Relative free energies for hydration of monovalent ions from QM and QM/MM simulations. *J. Chem. Theory Comput.* 9:4165–4175. http://dx.doi.org/10.1021/ct400296w

Li, Y., O.S. Andersen, and B. Roux. 2010. Energetics of double-ion occupancy in the gramicidin A channel. *J. Phys. Chem. B.* 114:13881–13888. http://dx.doi.org/10.1021/jp105820u

Light, P.E., C. Bladen, R.J. Winkfein, M.P. Walsh, and R.J. French. 2000. Molecular basis of protein kinase C-induced activation of ATP-sensitive potassium channels. *Proc. Natl. Acad. Sci. USA.* 97: 9058–9063. http://dx.doi.org/10.1073/pnas.160068997

MacKerell, A.D., D. Bashford, M. Bellott, R.L. Dunbrack, J.D. Evanseck, M.J. Field, S. Fischer, J. Gao, H. Guo, S. Ha, et al. 1998. All-atom empirical potential for molecular modeling and dynamics studies of proteins. *J. Phys. Chem. B.* 102:3586–3616.

Margolskee, R.F., B. McHendry-Rinde, and R. Horn. 1993. Panning transfected cells for electrophysiological studies. *Biotechniques.* 15:906–911.

McCleskey, E.W., and W. Almers. 1985. The Ca channel in skeletal muscle is a large pore. *Proc. Natl. Acad. Sci. USA.* 82:7149–7153. http://dx.doi.org/10.1073/pnas.82.20.7149

McCusker, E.C., C. Bagnéris, C.E. Naylor, A.R. Cole, N. D'Avanzo, C.G. Nichols, and B.A. Wallace. 2012. Structure of a bacterial voltage-gated sodium channel pore reveals mechanisms of opening and closing. *Nat Commun.* 3:1102. http://dx.doi.org/10.1038/ncomms2077

Meech, R.W., and G.O. Mackie. 1993. Potassium channel family in giant motor axons of Aglantha digitale. *J. Neurophysiol.* 69:894–901.

Moczydlowski, E., S.S. Garber, and C. Miller. 1984. Batrachotoxin-activated Na^+ channels in planar lipid bilayers. Competition of tetrodotoxin block by Na^+. *J. Gen. Physiol.* 84:665–686. http://dx.doi.org/10.1085/jgp.84.5.665

Morais-Cabral, J.H., Y. Zhou, and R. MacKinnon. 2001. Energetic optimization of ion conduction rate by the K^+ selectivity filter. *Nature.* 414:37–42. http://dx.doi.org/10.1038/35102000

Nonner, W., and B. Eisenberg. 1998. Ion permeation and glutamate residues linked by Poisson-Nernst-Planck theory in L-type calcium channels. *Biophys. J.* 75:1287–1305. http://dx.doi.org/10.1016/S0006-3495(98)74048-2

Nonner, W., D.P. Chen, and B. Eisenberg. 1998. Anomalous mole fraction effect, electrostatics, and binding in ionic channels. *Biophys. J.* 74:2327–2334. http://dx.doi.org/10.1016/S0006-3495(98)77942-1

Noskov, S.Y., and B. Roux. 2008. Control of ion selectivity in LeuT: two Na^+ binding sites with two different mechanisms. *J. Mol. Biol.* 377:804–818. http://dx.doi.org/10.1016/j.jmb.2008.01.015

Noskov, S.Y., S. Bernèche, and B. Roux. 2004. Control of ion selectivity in potassium channels by electrostatic and dynamic properties of carbonyl ligands. *Nature.* 431:830–834. http://dx.doi.org/10.1038/nature02943

Patlak, C.S. 1960. Derivation of an equation for the diffusion potential. *Nature.* 188:944–945. http://dx.doi.org/10.1038/188944b0

Payandeh, J., T. Scheuer, N. Zheng, and W.A. Catterall. 2011. The crystal structure of a voltage-gated sodium channel. *Nature.* 475:353–358. http://dx.doi.org/10.1038/nature10238

Payandeh, J., T.M. Gamal El-Din, T. Scheuer, N. Zheng, and W.A. Catterall. 2012. Crystal structure of a voltage-gated sodium channel in two potentially inactivated states. *Nature.* 486:135–139.

Rapaport, D.C. 2004. The art of Molecular Dynamics Simulation. Second edition. Cambridge University Press, Cambridge. 549 pp.

Ravindran, A., H. Kwiecinski, O. Alvarez, G. Eisenman, and E. Moczydlowski. 1992. Modeling ion permeation through batrachotoxin-modified Na^+ channels from rat skeletal muscle with a multi-ion pore. *Biophys. J.* 61:494–508. http://dx.doi.org/10.1016/S0006-3495(92)81854-4

Ren, D., B. Navarro, H. Xu, L. Yue, Q. Shi, and D.E. Clapham. 2001. A prokaryotic voltage-gated sodium channel. *Science.* 294:2372–2375. http://dx.doi.org/10.1126/science.1065635

Tang, S., G. Mikala, A. Bahinski, A. Yatani, G. Varadi, and A. Schwartz. 1993. Molecular localization of ion selectivity sites within the pore of a human L-type cardiac calcium channel. *J. Biol. Chem.* 268:13026–13029.

Thompson, A.N., I. Kim, T.D. Panosian, T.M. Iverson, T.W. Allen, and C.M. Nimigean. 2009. Mechanism of potassium-channel selectivity revealed by Na^+ and Li^+ binding sites within the KcsA pore. *Nat. Struct. Mol. Biol.* 16:1317–1324. http://dx.doi.org/10.1038/nsmb.1703

Treptow, W., and M.L. Klein. 2012. Computer simulations of voltage-gated cation channels. *J. Phys. Chem. Lett.* 3:1017–1023. http://dx.doi.org/10.1021/jz300089g

Yang, J., P.T. Ellinor, W.A. Sather, J.F. Zhang, and R.W. Tsien. 1993. Molecular determinants of Ca^{2+} selectivity and ion permeation in L-type Ca^{2+} channels. *Nature.* 366:158–161. http://dx.doi.org/10.1038/366158a0

Yu, H.B., S.Y. Noskov, and B. Roux. 2010. Two mechanisms of ion selectivity in protein binding sites. *Proc. Natl. Acad. Sci. USA.* 107:20329–20334. http://dx.doi.org/10.1073/pnas.1007150107

Yue, D.T., and E. Marban. 1990. Permeation in the dihydropyridine-sensitive calcium channel. Multi-ion occupancy but no anomalous mole-fraction effect between Ba^{2+} and Ca^{2+}. *J. Gen. Physiol.* 95:911–939. http://dx.doi.org/10.1085/jgp.95.5.911

Yue, L., B. Navarro, D. Ren, A. Ramos, and D.E. Clapham. 2002. The cation selectivity filter of the bacterial sodium channel, NaChBac. *J. Gen. Physiol.* 120:845–853. http://dx.doi.org/10.1085/jgp.20028699

Zhang, X., W. Ren, P. DeCaen, C. Yan, X. Tao, L. Tang, J. Wang, K. Hasegawa, T. Kumasaka, J. He, et al. 2012. Crystal structure of an orthologue of the NaChBac voltage-gated sodium channel. *Nature.* 486:130–134.